Journal of Ceramic Processing Research. Vol. 24, No. 6, pp. 992~1000 (2023)
(Received 19 September 2023, Received in revised form 12 November 2023, Accepted 16 November 2023)
https://doi.org/10.36410/jcpr.2023.24.6.992

J O U R N A L O F
Ceramic Processing Research

A study on microstructural and dielectric properties of $Ba_{0.5-x}Zn_xSr_{0.45}Ca_{0.05}TiO_3$ ceramics

Ying-Chieh Lee[a,b,*], Hui-Ju Hsu[c], I-Yu Huang[b], Huei-Jyun Shih[a] and Christian Pithan[d]
[a]*Institute of Precision Electronic Components, National Sun Yat-sen University, Kaohsiung 804, Taiwan*
[b]*Department of Electrical Engineering, National Sun Yat-sen University, Kaohsiung 804, Taiwan*
[c]*Department of Materials Engineering National Pingtung University of Technology and Science, Taiwan*
[d]*Peter Grunberg Institut, PGI-7 Electronic Materials, Forschungszentrum Julich GmbH, D-52425 Julich, Germany*

In this study, high entropy ceramics, specifically $Ba_{0.5-x}Zn_xSr_{0.45}Ca_{0.05}TiO_3$ (BZSCT), were synthesized using a solid-state reaction process and sintered at temperatures ranging from 1150 °C to 1250 °C. The properties of these ceramics were found to be significantly affected by variations in the Zn content. Densification of the BZSCT ceramics was observed to occur at sintering temperatures exceeding 1225 °C. Notably, the crystalline phases and dielectric properties of these ceramics were strongly influenced by the Zn content. Three distinct secondary phases were identified in the BZSCT ceramics, including $BaZn_{2.03}Ti_{3.93}O_{10.89}$, $Ba_2ZnTi_5O_{13}$ and Zn_2TiO_4. The addition of Zn resulted in a shift of the Curie point to lower temperatures. Specifically, with Zn substitution (up to 15 at.%), a Curie point of -60 °C was observed in the BZSCT ceramics. These ceramics exhibited a high dielectric constant of 1035, a low dielectric loss of 0.017%, and an impressive Q value of 442 when sintered at 1225 °C. Moreover, when comparing the dielectric constants of BZSCT ceramics at 1 MHz and 1 GHz, it was noted that the permittivity was only slightly reduced by less than 30% at lower frequencies. In contrast, the permittivity of BST ceramics decreased significantly, by approximately 70%, at microwave frequencies. These findings highlight the unique properties and potential applications of BZSCT ceramics, particularly in microwave applications where they outperform traditional BST ceramics.

Keywords: Microwave dielectric properties, $Ba_{0.5-x}Zn_xSr_{0.45}Ca_{0.05}TiO_3$, High Entropy Ceramics, Secondary phase.

Introduction

Barium strontium titanate (BST) has been a subject of significant scientific and technological interest for many years due to its unique dielectric properties. It possesses a remarkable combination of characteristics that allow for the realization of high dielectric constants and low dielectric losses simultaneously [1-4]. These properties make BST particularly attractive for practical microwave ceramics. Microwave ceramics used in practical applications typically require specific features such as intermediate values of the dielectric constant, low dielectric loss, large tunability, and excellent dielectric thermal stability [5-7]. BST ceramics fulfill these requirements effectively. It is widely known that the Curie temperature of BST, specifically $Ba_{0.5}Sr_{0.5}TiO_3$, is approximately 250 K [8, 9]. Consequently, BST ceramics intended for microwave applications typically undergo a transition from the ferroelectric to the paraelectric state at temperatures well below room temperature [10]. This behavior is due to BST's paraelectric nature at room temperature, which, coupled with its high dielectric tunability and relatively low loss at microwave frequencies, makes it an ideal material for microwave applications [11, 12].

Extensive research has been conducted on high-entropy ceramics (HECs), which are derived from multicomponent ceramic compounds such as metallic oxides, nitrides, or carbides. These HECs exhibit the potential to form a single-phase solid solution, both in bulk and film forms [13-15]. The development of single-phase HECs has been driven by the belief that they possess advantageous mechanical properties due to significant lattice distortions and sluggish diffusion behavior. These characteristics make HECs suitable for applications that require high mechanical performance and phase stability at elevated temperatures [16, 17]. Numerous studies have reported the successful processing and fabrication of HECs using metallic oxides, borides, carbides, or nitrides [18-20]. The notable enhancement in mechanical performance observed in HECs is generally attributed to the strengthening mechanism of the solid solution. However, it is worth noting that, to date, no publications have reported on HECs with the ABO_3 perovskite structure. Most studies on HECs have primarily focused on phase

*Corresponding author:
Tel : +886-7-5252-000
Fax: +886-7-5254-199
E-mail: yc56@mail.nsysu.edu.tw

transformations and mechanical performance, without exploring their potential within the ABO_3 perovskite structure.

The ferroelectric compound $BaTiO_3$, with its perovskite-type crystal lattice structure ABO_3, demonstrates exceptional chemical and crystallographic adaptability. It exhibits a remarkable capacity to incorporate a wide range of metallic species as dopants or substitutional additions on either the A-site or B-site. This flexibility enables significant modifications in the ionic size, valence state, and concentration of the substituting species, thereby facilitating the formation of extensive solid solutions. Additionally, aliovalent substitutions have the potential to compensate for electronic disorder or lattice point defects, including electrons, holes, or vacancies [21-23].

This study aimed to design and synthesize a new high-entropy ceramic, $Ba_{0.5-x}Zn_xSr_{0.45}Ca_{0.05}TiO_3$ (x=0.05, 0.10, and 0.15), with a perovskite structure using solid-state processing. The high-entropy phase was characterized and evaluated through electron microscopy and X-ray diffraction (XRD) analysis. The investigation focused on understanding the mechanism of Zn and Ca substitution, exploring the microwave dielectric properties, and examining the microstructures of the $Ba_{0.5-x}Zn_xSr_{0.45}Ca_{0.05}TiO_3$ high-entropy ceramic.

Experimental Procedure

$Ba_{0.5-x}Zn_xSr_{0.45}Ca_{0.05}TiO_3$ ceramics (x=0.05, 0.10, and 0.15) were prepared by solid oxide reaction. Stoichiometric titanium oxide (99.9%), barium carbonate (99.8%), strontium carbonate (99.9%), calcium carbonate (99.0%) and zinc oxide (99.9) powders were used as raw materials. To easy arrange the samples, $Ba_{0.45}Zn_{0.05}Sr_{0.45}Ca_{0.05}TiO_3$ ceramics is called BZSCT-9191, $Ba_{0.4}Zn_{0.1}Sr_{0.45}Ca_{0.05}TiO_3$ ceramics is called BZSCT-8291 and $Ba_{0.35}Zn_{0.15}Sr_{0.45}Ca_{0.05}TiO_3$ ceramics is called BZSCT-7391.

The mixtures were ball-milled, dried and calcined at 1100 °C for 2 h to get the BZSCT powders. To homogenize the powders, a mortar and pestle were employed along with ethanol as a medium. The resulting mixtures were further processed in a planetary ball mill utilizing yttria-stabilized zirconia balls, operating at 90 rpm for a duration of 24 hours. Following this, the powders were combined with a binder additive, namely polyvinyl alcohol (PVA), and pressed into disk-shaped samples or pellets. The resulting pellets were then subjected to sintering in air, with temperatures ranging from 1150 °C to 1250 °C for a duration of 2 hours, utilizing a heating rate of 5 °C/min. Finally, the samples were cooled within the furnace. It is important to note that the average particle size of the initial powders after grinding was determined to be 5 ± 0.5 μm.

The identification of crystalline phases in the sintered ceramics was conducted through X-ray diffraction pattern analysis (XRD) using a Bruker D8A instrument from Germany. Cu-Kα radiation was employed, and the analysis covered a 2θ range of 20 to 80 degrees. The diffraction spectra were collected at a scan rate of 2 degrees per minute. The lattice parameters were determined using the DIFFRAC plus TOPAS version 3.0 program. Microstructural observations of the sintered ceramics were carried out using a scanning electron microscope (SEM) model JEOL JEL-6400 from Japan, in conjunction with energy-dispersive spectroscopy (EDS). Additionally, the bulk density of the sintered pellets was measured using the Archimedes method.

For dielectric property measurement, disc capacitors were fabricated by applying silver electrodes on both sides of the samples. The electrodes were dried and then fired at a temperature of 600 ºC for a duration of 10 minutes. The dielectric behavior at microwave frequencies was assessed using the TE01δ shielded cavity method, employing a network analyzer (8720ES, Agilent, Palo Alto, CA) and a temperature chamber (Delta 9023, Delta Design, Poway, CA). The temperature coefficient of frequency (τf) was calculated using the following formula:

$$\tau_f = (f_{85} - f_{25}) / [f_{25} \times (85–25)]$$

where f_{85} and f_{25} are the $TE_{01\delta}$ resonant frequencies at 85 ºC and 25 ºC, respectively. Δf is ($f_{85} - f_{25}$), the variation of resonant frequency (GHz) and ΔT is (85 ºC-25 ºC), the temperature range (°C)

Results and Discussion

Phase and microstructure of $Ba_{0.5-x}Zn_xSr_{0.45}Ca_{0.05}TiO_3$ ceramics

Three distinct specimens were prepared in this study, denoted as BZSCT-9191, BZSCT-8291, and BZSCT-7391. These specimens represent a significant advancement in the field of High-Entropy Ceramics (HECs). A novel high-entropy ceramic composite incorporating BaO, ZnO, SrO, CaO, and TiO_2 was meticulously engineered and synthesized in situ, with subsequent consolidation through solid-state processing [24]. Fig. 1 displays the XRD patterns of BZSCT-9191, BZSCT-8291, and BZSCT-7391 ceramics, all sintered at a temperature of 1225 °C. An in-depth analysis of the phase composition reveals a noteworthy achievement: BZSCT-9191 ceramics exhibit the formation of essentially a single-phase $Ba_{0.5}Sr_{0.5}TiO_3$ without the presence of secondary phases. In contrast, BZSCT-7391 ceramics sintered at the same temperature display significant secondary phases, specifically $BaZn_{2.03}Ti_{3.93}O_{10.89}$ and Zn_2TiO_4. The reflection peaks observed in the samples have been successfully indexed to a cubic perovskite structure, demonstrating excellent agreement with standard data (JCPD: 39-1395). The lattice constant was precisely

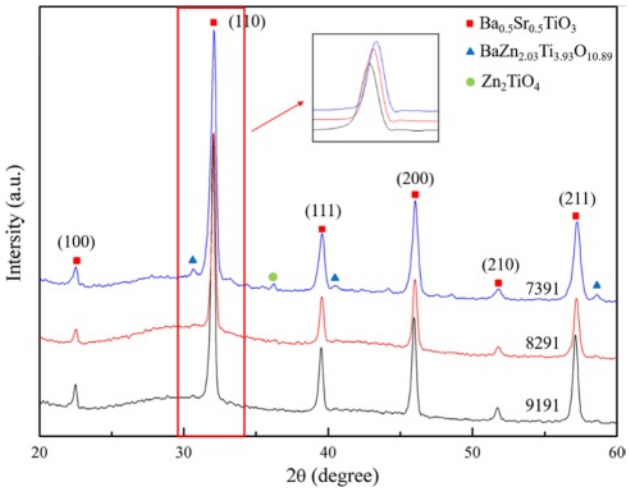

Fig. 1. XRD patterns of BZSCT-9191, -8291, -7391 ceramics sintered at 1225 °C.

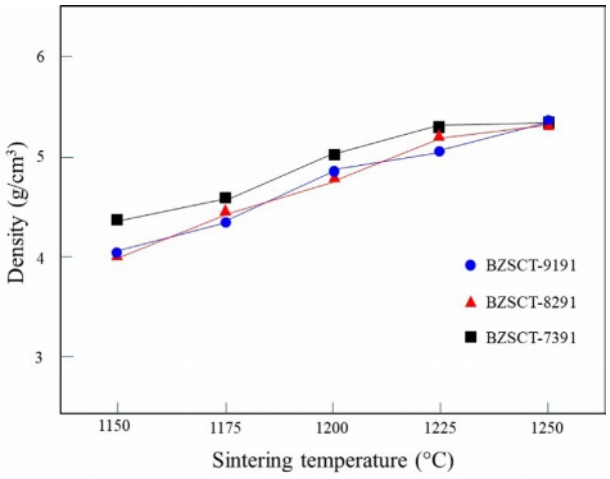

Fig. 2. The bulk density of BZSCT ceramics sintered at ranging from 1150 °C to 1250 °C.

determined to be a=3.9471 Å. It is well-established that in the temperature range below 1350 °C, the binary system $BaTiO_3$-ZnO primarily comprises $BaTiO_3$ and ZnO as the sole detected crystalline phases [25, 26]. Furthermore, previous studies have reported the limited solubility of ZnO in $BaTiO_3$, which is less than 2 mol%. To further investigate potential shifts in XRD peaks, a focused examination was conducted by narrowing down the XRD spectra to a 2θ range of 31 ° to 35 °. It is evident that the (110) peak of the $Ba_{0.5}Sr_{0.5}TiO_3$ phase has shifted to higher angles for both BZSCT-8291 and BZSCT-7391 ceramics. This shift in peak positions can be attributed to the substitution of Zn^{2+} for Ti^{4+} in the primitive cell of $BaSrTiO_3$ [27]. Notably, the ionic radii of Ba^{2+}, Sr^{2+}, Ca^{2+}, Ti^{4+}, and Zn^{2+} are approximately 1.61 Å, 1.44 Å, 1.34 Å, 0.605 Å, and 0.75 Å, respectively. As a result, Zn^{2+} may occupy the Ti^{4+} site in the $BaSrTiO_3$ primitive cell, leading to an expansion of the primitive cell. However, Zn^{2+} acts as acceptors, introducing oxygen vacancies to maintain electroneutrality. Consequently, the lattice constant decreases when oxygen vacancies are generated in the BZSCT ceramics. This substitution-induced decrease in lattice constants is responsible for the observed shift of the peaks towards higher angles. These findings not only underscore the successful synthesis of high-entropy ceramics with single-phase characteristics but also provide valuable insights into the structural modifications induced by Zn incorporation,

When Zn^{2+} substitutes Ti^{4+} cations on the B site, a double ionized oxygen vacancy is formed simultaneously, i.e.

$$ZnO \rightarrow Zn_{Ti}'' + V_o^{\bullet\bullet} + O_o \quad (1)$$

The BZSCT ($Ba_{0.5-x}Zn_xSr_{0.45}Ca_{0.05}TiO_3$) ceramics in this study underwent sintering in an air atmosphere within a temperature range of 1150 to 1250 °C for a duration of 2 hours. Fig. 2 illustrates the bulk density of the BZSCT ceramics as a function of the sintering temperatures. As the sintering temperature increased, the density of the BZSCT ceramics exhibited a progressive rise, reaching its peak value at 1225 °C. Specifically, the maximum bulk densities achieved for BZSCT-9191, -8291, and -7391 were 5.06, 5.20, and 5.32 g/cm^3, respectively. It is noteworthy that the BZSCT-9191 sample achieved approximately 95% of the theoretical density of $Ba_{0.5}Sr_{0.5}TiO_3$ [28].

A notable comparison between the sintering temperatures of BMSCT ($Ba_{0.5-x}Mg_xSr_{0.45}Ca_{0.05}TiO_3$) and BZSCT ceramics reveals a significant difference. While BMSCT-9191 ceramics require sintering at 1350 °C [29], BZSCT-9191 ceramics can achieve densification at a notably lower temperature of 1225 °C. This phenomenon can be attributed to the introduction of ZnO in BZSCT ceramics, which leads to a reduction in sintering temperatures. This reduction can be rationalized by the substitution of B-site Ti^{4+} ions with Zn^{2+} ions at the given temperature. To maintain charge neutrality in the system, it is plausible to suggest the formation of Zn^{2+} interstitials or oxygen vacancies.

The linear shrinkage of the BZSCT ceramics as a function of sintering temperatures is depicted in Fig. 3. It is evident that the linear shrinkage increases with the elevation of the sintering temperature, with the temperature at which larger shrinkage begins being 1080 °C for BZSCT-7391 and 1130 °C for BZSCT-9191 and -8291, respectively. Numerous prior studies have consistently highlighted the significant impact of ZnO on the dielectric performance, microstructure, and sintering behavior of $BaTiO_3$. ZnO plays a pivotal role in enhancing density by facilitating controlled grain growth of $BaTiO_3$, while simultaneously reducing dielectric losses through substitution [30-32].

The SEM micrographs in Fig. 4 illustrate the microstructure of BZSCT ceramics sintered at 1225 °C. It is evident that significant densification occurs at this

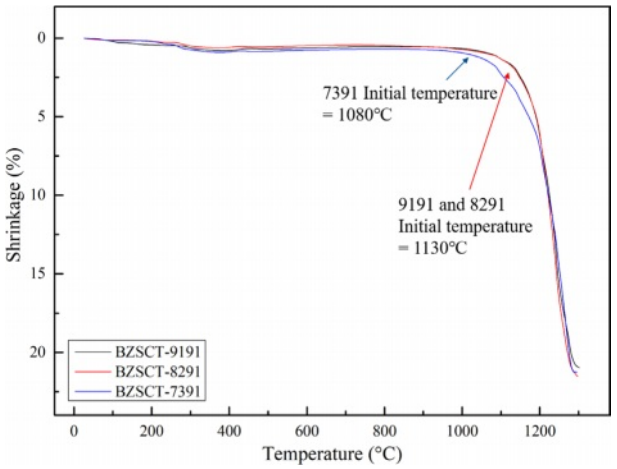

Fig. 3. Thermal analysis curve graph of BZSCT-9191, -8291, -7391 powders.

sintering temperature. The grain size of the BZSCT-9191, -8291, and -7391 ceramics sintered at 1225 °C measures 3.50 μm, 3.01 μm, and 2.28 μm, respectively. The determination of grain size was accomplished using the linear intercept method, involving the drawing of three straight lines on the SEM images. Notably, there is a discernible trend of decreasing grain size with the addition of ZnO.

Traditionally, Zn doping has been associated with grain growth in Barium Strontium Titanate (BST) ceramics, and the inclusion of ZnO in ceramic $BaTiO_3$ has been reported to increase the density and grain size of the sintered bodies [33]. However, the findings from this study suggest a different scenario, where the addition of ZnO appears to suppress grain growth. This behavior indicates that zinc functions as an acceptor-type dopant at grain boundaries in the context of this study. Comparing the grain sizes of specimens between BMSCT ceramics sintered at 1350 °C and BZSCT ceramics sintered at 1225 °C, it is evident that the grain sizes for BMSCT and BZSCT are 2.4 μm and 3.5 μm, respectively [29]. This discrepancy can be attributed to the distinct processing conditions of the BZSCT ceramics. Specifically, the BZSCT ceramics are processed through sintering of powder compacts with the presence of liquid phases at the elevated temperature of 1225 °C.

Detailed microstructural analysis of BZSCT-9191 ceramics sintered at 1225 °C was conducted using Transmission Electron Microscopy (TEM), as depicted in Fig. 5. Fig. 5(a) presents TEM images captured from different positions within the specimens, while Fig. 5(b), 5(c), and 5(d) show the corresponding electron diffraction patterns. The electron diffraction patterns revealed that matrix grains corresponded to the $Ba_{0.5}Sr_{0.5}TiO_3$ phase, as demonstrated in Fig. 5(b). Additionally, secondary phase grains were identified as belonging to the $BaZn_{2.03}Ti_{3.93}O_{10.89}$ phase, as shown in Fig. 5(c). Furthermore, another secondary phase was

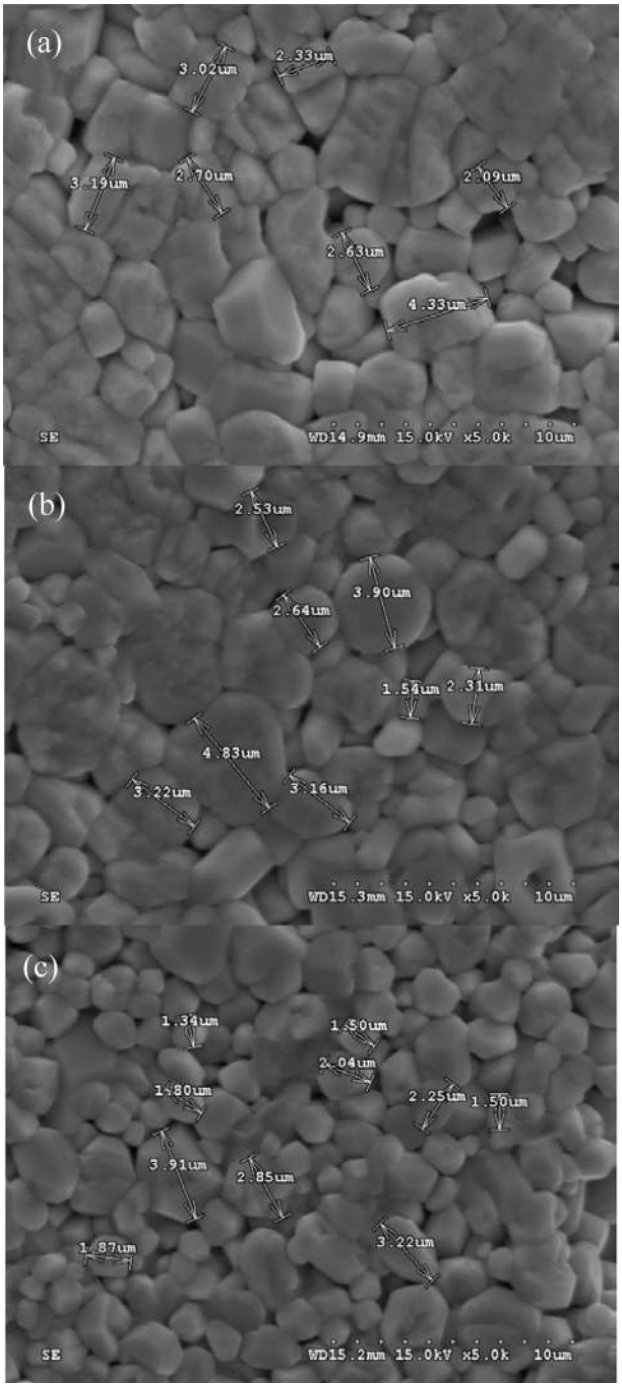

Fig. 4. SEM micrographs of BZSCT ceramics sintered at 1225 °C (a) 9191 (b) 8291 (c) 7391.

observed at the triple junctions of the $Ba_{0.5}Sr_{0.5}TiO_3$ (BST) grains, which was identified as $Ba_2ZnTi_5O_{13}$, as illustrated in Fig. 5(d). The refined lattice parameters for the $Ba_2ZnTi_5O_{13}$ compound were determined to be a= 15.2822 Å, b=3.8977 Å, c=9.1398 Å, β=98.769°, and Z=2 [34]. These findings suggest that the incorporation of ZnO into the BST structure is constrained by its solubility at elevated temperatures. Due to the relatively smaller ionic radius of Zn^{2+} compared to the A-site cations, ZnO tends to selectively replace Ti^{4+} ions,

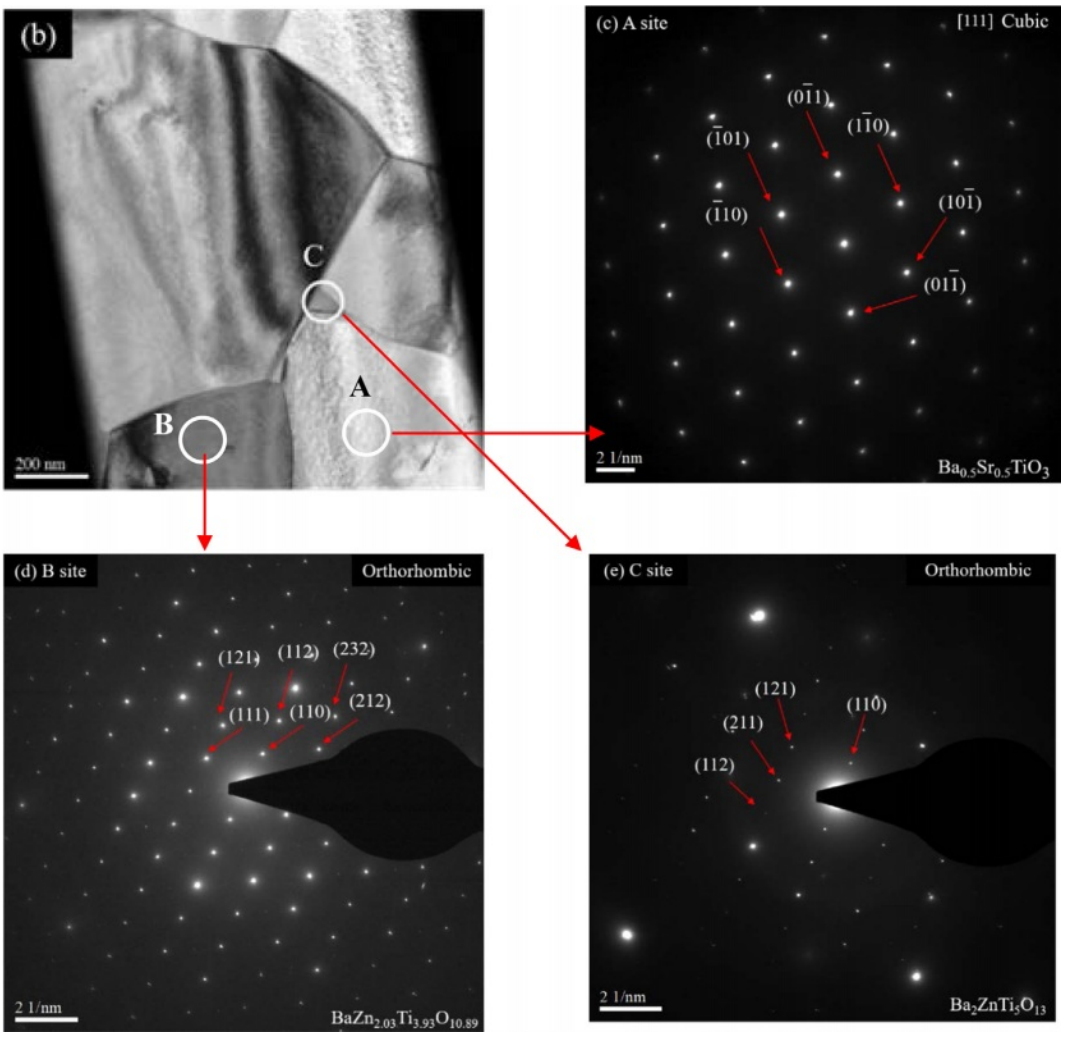

Fig. 5. TEM micrographs of BZSCT-9191 ceramics sintered at 1225 °C (a) TEM microstructure (b) selected-area electron diffraction of A position (c) selected-area electron diffraction of B position (d) selected-area electron diffraction of C position.

aligning with previous research on the topic [35].

Additionally, TEM analysis was performed on BZSCT-8291 ceramics sintered at 1225 °C, as displayed in Fig. 6. Fig. 6(a) exhibits TEM images from different positions within the specimens, while Fig. 6(b), (c), and (d) show the corresponding electron diffraction patterns. The analysis of electron diffraction patterns revealed that positions A, B, and C corresponded to the phases $Ba_{0.5}Sr_{0.5}TiO_3$, $BaZn_{2.03}Ti_{3.93}O_{10.89}$, and Zn_2TiO_4, respectively, as depicted in Fig. 6(b), (c), and (d). It is evident that the primary phase in these ceramics was the $Ba_{0.5}Sr_{0.5}TiO_3$ phase, with secondary phases identified as $BaZn_{2.03}Ti_{3.93}O_{10.89}$ and Zn_2TiO_4. The orthotitanate Zn_2TiO_4 was found to possess a spinel structure with a space group of Fd-3m, where Zn^{2+} cations occupy the 8a and 16d sites, Ti^{4+} cations occupy the 16d sites, and oxygen occupies the 32e site [36]. Furthermore, the formation of Zn_2TiO_4 can occur when the ZnO-TiO_2 solid solution reaches a stoichiometric (2:1 mol%) ratio [37]. It is noteworthy that the secondary phases observed in BZSCT-9191 and BZSCT-8291 ceramics were $Ba_2ZnTi_5O_{13}$ and Zn_2TiO_4, respectively. This variation may be attributed to the higher ZnO content in the BZSCT specimens, which promotes the formation of the Zn_2TiO_4 phase. This can be explained by the excess ZnO present in the grain boundaries. In situations where excessive ZnO exists, Ti^{4+} may segregate towards the grain boundaries when substituted by Zn^{2+}, and Zn^{2+} will precipitate into the grain boundaries when significant lattice distortion occurs.

Furthermore, the solubility limit of Zn in BST is limited to less than 2.0 mol%. Excess ZnO in the BZSCT ceramics system can lead to the formation of the Zn_2TiO_4 secondary phase at 1225 °C [38]. The study highlights that BZSCT ceramics do not retain a single-phase state at elevated temperatures. Instead, the formation or transformation of phases depends on atomic diffusion, necessitating coordinated migration of cations and anions to achieve equilibrium among the participating phases. In situations with numerous

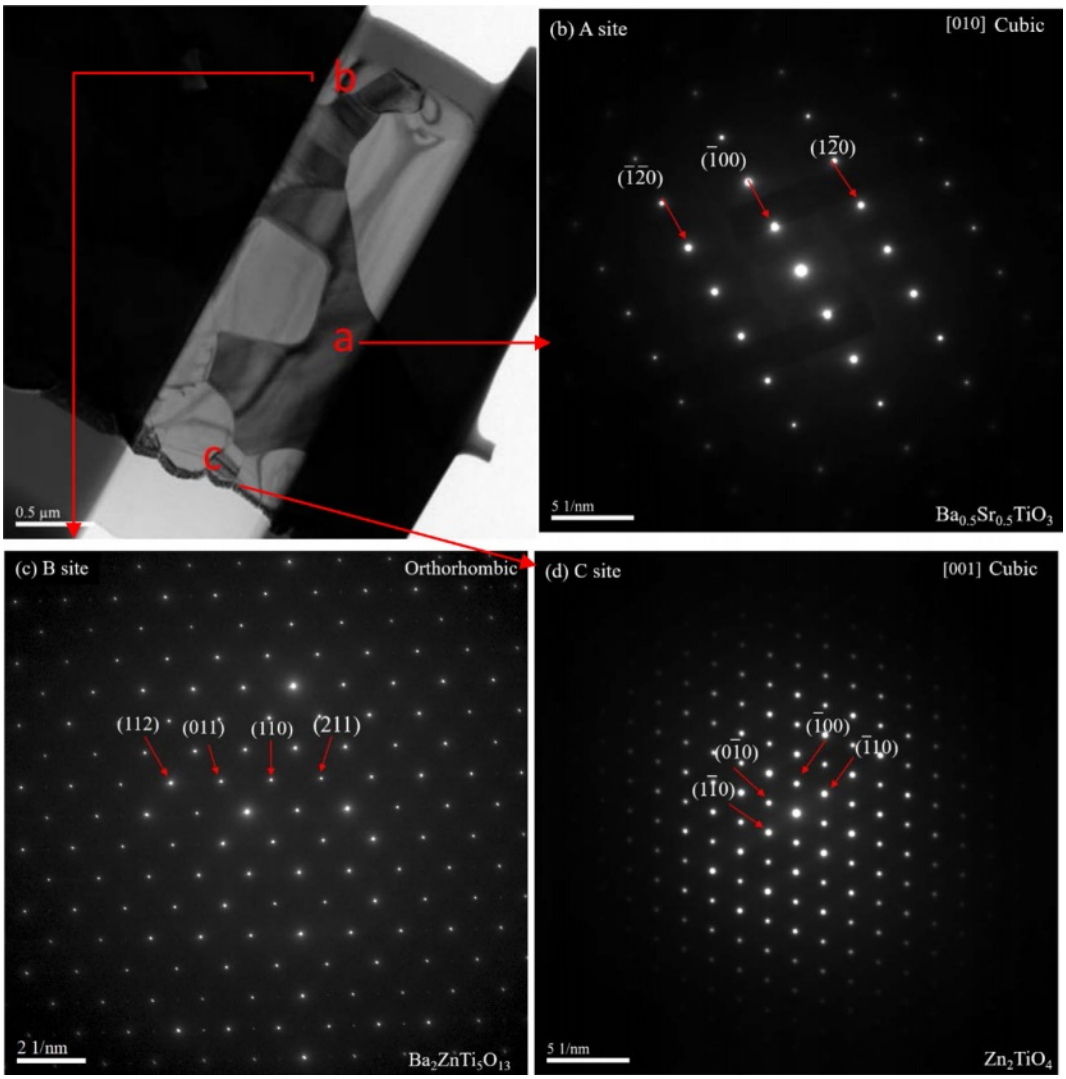

Fig. 6. TEM micrographs of BZSCT-8291 ceramics sintered at 1225 °C (a) TEM microstructure (b) selected-area electron diffraction of A position (c) selected-area electron diffraction of B position (d) selected-area electron diffraction of C position.

substituting cations and a high concentration, such as in high-entropy ceramics (HECs) [39], the extensive formation of solid solutions may hinder atomic mobility and potentially limit effective diffusion rates.

Dielectric properties of $Ba_{0.5-x}Zn_xSr_{0.45}Ca_{0.05}TiO_3$ ceramics

Figure 7 illustrates the correlation between temperature and fixed frequency permittivity data at 1 MHz for specimens sintered at a temperature of 1225 °C. The Curie temperature (Tc) values for BZSCT-9191, -8291, and -7391 ceramics are -35 °C, -48 °C, and -60 °C, respectively. It is noteworthy that an incremental change in the Curie point becomes apparent as the value of 'x' increases. Specifically, elevating the 'x' value from 0.05 to 0.15 results in variations in the grain size of the specimens sintered at 1225 °C. This phenomenon can be attributed to the increase in Zn content, which implies a reduction in the Ba content and a proportional rise

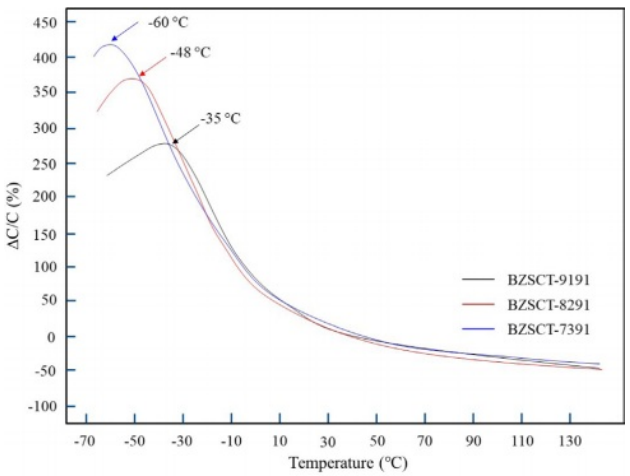

Fig. 7. The dielectric properties of BZSCT ceramics sintered at 1225 °C (a) permittivity and (b) dielectric loss. (measured at 1 MHz).

in Sr content. Consequently, the Ba/Sr ratio decreases within the $Ba_{0.5-x}Zn_xSr_{0.45}Ca_{0.05}TiO_3$ system.

Barium Strontium Titanate (BST) belongs to the perovskite family, featuring an ABX3 crystal structure. It shares crystalline characteristics with typical perovskites, primarily exhibiting a cubic nature. Its chemical formula is represented as ($Ba_{1-x}Sr_xTiO_3$) [40, 41]. Above the Curie temperature, BST compounds experience a transition from the ferroelectric phase to the paraelectric phase, characterized by a cubic crystal structure [42] $Ba_{1-x}Sr_xTiO_3$ demonstrates both tetragonal and cubic phases, with their presence being contingent on the Ba/Sr ratio and temperature conditions. It is observed that the ferroelectric state (tetragonal phase) prevails below the Curie temperature, while the paraelectric state (cubic phase) manifests above the Curie temperature [43]. Therefore, it is reasonable to infer that the introduction of more Zn leads to a shift in the Curie point towards lower temperatures.

The dielectric properties of BZSCT ceramics were investigated with respect to sintering temperatures and zinc oxide (ZnO) content at a frequency of 1 MHz, as depicted in Fig. 8(a). Notably, the dielectric constant exhibited an upward trend as sintering temperatures increased within the range of 1150 °C to 1250 °C. This behavior mirrors the relationship observed between bulk density and sintering temperatures. Importantly, it was observed that the dielectric constant significantly decreased with an increase in ZnO content within the BZSCT ceramics. For instance, the dielectric constant (εr) values for BZSCT-9191, -8291, and -7391 ceramics sintered at 1225 °C were measured as 1195, 1035, and 735, respectively. Comparatively, the dielectric constant of pure BST ceramic at 1350 °C was 1650, surpassing that of the BZSCT ceramics. This decrease in dielectric constant in BST ceramics is likely attributed to the restriction of grain growth induced by Zn doping.

It is worth noting that the addition of calcium in BST ceramics can also lead to a reduction in the dielectric constant. A study by Hanting Dong et al. [44] investigated the effects of calcium additions and various addition methods on the microstructure, dielectric properties, and tunability of BSCT ceramics. They observed a significant reduction in the dielectric constant, from approximately 2800 to around 1500, upon the incorporation of calcium. Furthermore, the presence of secondary phases in BZSCT ceramics, as indicated in this study, has a substantial impact on the dielectric constant [45, 46].

Figure 8(b) illustrates the variations in dielectric loss observed across the BZSCT ceramics sintered within a temperature range of 1150 °C to 1250 °C. The dielectric loss decreased with increasing sintering temperatures, reaching a minimum at 1225 °C, followed by a sudden increase at 1250 °C. For BZSCT-9191, -8291, and -7391 ceramics sintered at 1225 °C, the dielectric loss values were measured as 2.2×10^{-3}, 1.7×10^{-3}, and 1.5

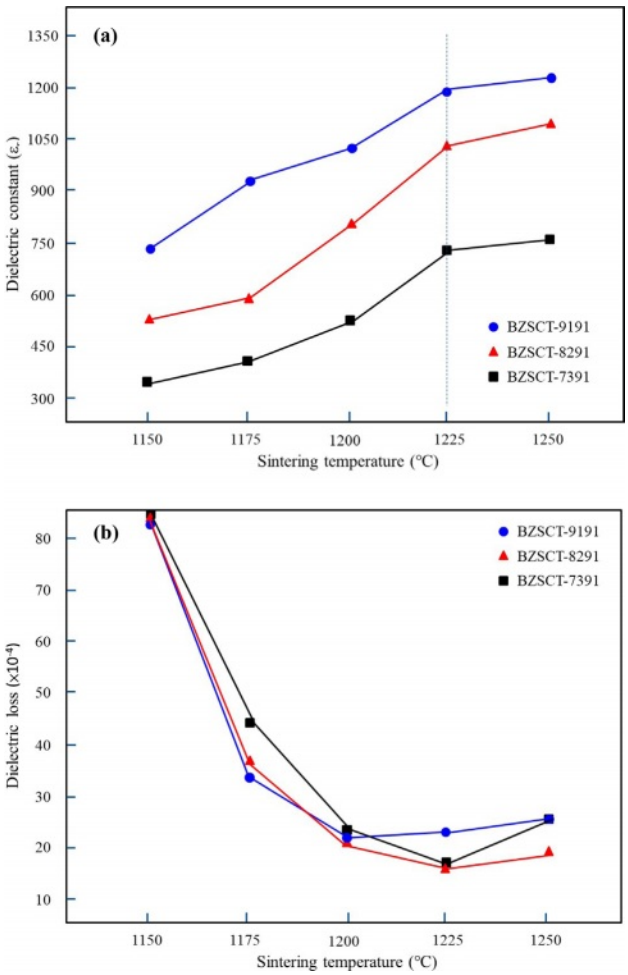

Fig. 8. Temperature coefficient of capacitance for BZSCT ceramics sintered at 1225 °C.

$\times10^{-3}$, respectively. In comparison to pure BST, which exhibited a dielectric loss of 1.3×10^{-3} [29], the dielectric loss of BST was lower than that of BZSCT ceramics. It is widely acknowledged that the presence of oxygen vacancies and other defects can contribute to increased dielectric losses. Therefore, to achieve the purest form of BST with minimal dielectric loss, efforts to mitigate such defects are essential.

Table 1 presents dielectric constant (ε_r) values of BZSCT ceramics sintered at 1225 °C, measured at room temperature and 1.3 GHz. Specifically, the ε_r values for BST, BZSCT-9191, BZSCT-9182, and BZSCT-7391 ceramics sintered at 1225 °C are 509, 896, 736, and 584, respectively. Notably, at this sintering temperature, BZSCT-9191 ceramics exhibit a significantly higher dielectric constant than the other ceramics at microwave frequencies. Comparing the dielectric constant values at 1 MHz and 1.3 GHz, we observe that the permittivity of BZSCT ceramics experiences a decrease of less than 30%, whereas the pure BST ceramics exhibit a drastic reduction of approximately 70% at microwave frequencies. This decrease is a well-known phenomenon in dielectric materials, where the dielectric constant

Table 1. Physical and dielectric properties of BZSCT ceramics sintered at 1225 °C.

BZSCT Smple	Density (g/cm^3)	Permittivity (1 MHz)	Insertion loss ($tan\times10^{-4}$)	Resonant Frequency (GHz)	Permittivity (Resonant Frequency)	Quality factor (GHz)	Insulation resistance (Ω)	TCF (ppm/°C)
BST	5.3	1644	13	1.3	509	323	5.3E+11	1109
9191	5.3	1195	22	1.32	896	378	7.1E+12	1614
8291	5.3	1035	17	1.39	736	442	4.9E+12	1819
7391	5.2	735	15	1.63	584	602	8.5E+12	3432

typically decreases with increasing frequency due to the reduction of space charge polarization effects. However, at lower frequencies, a higher dielectric constant is observed, attributed to the presence of space charge polarization at grain boundaries, creating a potential barrier [47].

The quality factor (Q factor) values for BST and BZSCT ceramics were also measured at room temperature and 1.3 GHz, as summarized in Table 1. For BST, BZSCT-9191, -8291, and -7391 ceramics sintered at 1225 °C, the Q factor values are 323, 378, 442, and 602, respectively. A higher Q factor indicates lower dielectric loss (Q = 1/tanδ). In this investigation, it is noteworthy that BZSCT-7391 ceramics exhibit the lowest Q value, implying the presence of more second phases in this material, as confirmed by XRD analysis (Fig. 1). One such phase, Zn_2TiO_4, is likely contributing to the higher Q value observed in BZSCT ceramics [48]. However, it is important to note that the temperature coefficient of resonant frequency (τ_f) values for BZSCT-9191, -8291, and -7391 ceramics at a sintering temperature of 1225 °C are 1641, 1891, and 3432, respectively. This outcome indicates that excessive ZnO addition in BZSCT ceramics leads to higher τ_f values.

Conclusions

We synthesized $Ba_{0.45}Zng_{0.05}Sr_{0.5-x}Ca_xTiO_3$ (x=0.05, 0.10 and 0.15) high entropy ceramics through a solid-state reaction method, followed by densification at 1225 °C. The introduction of zinc as an acceptor, replacing titanium on the B-site within the perovskite ABO3 structure, resulted in a notable shift of the Curie point to lower temperatures and a significant alteration in dielectric properties. This shift in properties can be attributed to the formation of three distinct secondary phases: $BaZn_{2.03}Ti_{3.93}O_{10.89}$, $Ba_2ZnTi_5O_{13}$ and Zn_2TiO_4 within the specimens. Additionally, in the case of BZSCT-9191 ceramics, the presence of the $Ba_2ZnTi_5O_{13}$ phase was observed in certain regions within the BST grains, leading to the formation of secondary phases at the triple-junction positions. Notably, BZSCT-8291 ceramics sintered at 1225 °C exhibited superior microwave dielectric properties, characterized by a permittivity of 736 and a Q factor of 442 at 1.3 GHz. Comparing the dielectric constants at 1 MHz and 1 GHz, it is evident that the permittivity of BZSCT ceramics experiences a modest decrease of less than 30% at lower frequencies. In contrast, pure BST ceramics exhibited a substantial reduction of approximately 70% at microwave frequencies. This behavior is in line with the typical trend of dielectric ceramics, where the dielectric constant decreases with increasing frequency, primarily due to the diminishing space charge polarization effects.

References

1. W. Chang and L. Sengupta, J. Appl. Phys. 92 (2002) 3941-3946.
2. U. Ozgur, Ya. Alivov, and H. Morkoc, J. Mater. Sci.: Mater. Electron. 20 (2009) 911-952.
3. I. Novianty, K.B. Seminar, Irzaman, and I.W. Budiastra, Earth and Environmental Science 187 (2018) 012077:1-7.
4. J. Huang, Y. Cao, and M.C. Hong, P. Du, Appl. Phys. Letters 92 (2008) 022911: 1-3.
5. T. Takada, S.F. Wang, S. Yoshikawa, S.J. Jang, and R.E. Newnham, J. Am. Ceram. Soc. 77 (1994) 1909.
6. F.T.Z. Toma, I.N. Esha, M. Al-Amina, M.N.I. Khan, and K.H. Maria, J. Ceram. Process. Res. 18[10] (2017) 701-710.
7. T.T. Khan, I.H. Kim, and S.C. Ur, J. Ceram. Process. Res. 19[4] (2018) 327-331.
8. W. Chang, J.S. Horwitz, A.C. Carter, J.M. Pond, S.W. Kirchoefer, C.M. Gilmore, and D.B. Chrisey, Appl. Phys. Lett. 74 (1999) 1033-1035.
9. A.E. Ghandouri, S. Sayouri, T. Lamcharfi, and L. Hajji, J. Ceram. Process. Res. 19[2] (2018) 154-170.
10. S. Nishigaki, H. Kato, S. Yano, and R. Kamimura, Am. Ceram. Soc. Bull. 66 (1987) 1405-1409.
11. J.H. Leach, H. Liu, V. Avrutin, B. Xiao, Ü. Özgür, H. Morkoç, J. Das, Y. Y. Song, and C. E. Patton, J. Appl. Phys. 107 (2010) 084511.
12. S.H. Lee, W.C. Song, J.M. Kim, and J.R. Yoon, J. Ceram. Process. Res. 18[3] (2017) 188-191.
13. S. Akrami, P. Edalati, M. Fuji, and K. Edalati, Mater. Sci. Eng. R Rep. 146 (2021) 100644.
14. R.Z. Zhang and M.J. Reece, J. Mater. Chem. A 7 (2019) 22148-22162.
15. K. Wang, L. Chen, C. Xu, W. Zhang, Z. Liu, Y. Wang, J. Ouyang, X. Zhang, Y. Fu, and Y. Zhou, J. Mater. Sci. Technol. 39 (2020) 99-105.
16. Y. Pu, Q. Zhang, R. Li, M. Chen, X. Du, and S. Zhou, Appl. Phys. Lett. 115 (2019) 223901.
17. W. Liu, F. Li, G. Chen, G. Li, H. Shi, L. Li, Y. Guo, J. Zhai, and C. Wang, J. Mater. Sci. 56 (2021) 18417-18429.

18. B. Cantor, I. Chang, P. Knight, and A. Vincent, Mater. Sci. Eng. A 375 (2004) 213-218.
19. E. Fazakas, V. Zadorozhnyy, L. Varga, A. Inoue, D. Louzguine-Luzgin, F. Tian, and L. Vitos, Int. J. Refractory Met. Hard Mater. 47 (2014) 131-138.
20. D. Bérardan, S. Franger, D. Dragoe, A.K. Meena, and N. Dragoe, Phys. Status Solidi RRL 10 (2016) 328-333.
21. R.J. Gambino and F.W. Leonhard, J. Am. Ceram. Soc. 44 (1961) 271-275.
22. H. Sözeri, I. Küçük, and H. Özkan, J. Magn. Magn. Mater. 323 (2011) 1799-1805.
23. J. Cen, B. Zhu, S.R. Kavanagh, and A.G. Squires, J. Mater. Chem. A 11 (2023) 13353-13370.
24. H. Xiang, Y. Xing, F. Z. Dai, H. Wang, L. Su, L. Miao, G. Zheng, Y. Wang, X. Qi, L. Yao, H. Wang, B. Zhao, J. Li, and Y. Zhou, J. Adv. Ceram. 10 (2021) 385-441.
25. R.S. Roth, C.J. Rawn, C.G. Lindsay, and W. Wong-Ng, J. Solid State Chem. 104 (1993) 99-118.
26. Z. Liu, Z. Xing, H. Wang, Z. Xue, S. Chen, G. Jin, and X. Cui, J. Alloys Comp. 727 (2017) 696-705.
27. S.K. Das, P.P. Rout, S.K. Pradhan, and B.K. Roul, Journal of Advanced Ceramics 1 (2012) 241-248.
28. H. Shin, T. Byun, and S.O. Yoon, J. Korean Ceram Soc. 49 (2012) 100-104.
29. C. Pithan, M.Y. Yeh, H.Y. Lee, Y.C. Lee, and D.F. Hennigs, Mater. Chem. Phys. 296 (2023) 127290, 1-11.
30. F. Gao, R. Hong, J. Liu, Z. Li, and C.S. Tian, Ceram. Int. 35 (2009) 1863-1869.
31. G.Y. Wang, Y. Qin, C. Jie, and Y.J. Wang, J. Fuel Chem. Technol. 38 (2010) 502-507.
32. G. Dong, S. Ma, J. Du, and J. Cui, Ceram. Int. 35 (2009) 2069-2075.
33. A.C. Caballero, Jr. F. FernBndez, C. Moure, and P. Duriin, Journal of the European Ceramic Society 17 (1997) 513-523.
34. V.N. Reddy, T.S. Sarmash, K.C. Babu Naidu, M. Maddaiah, and T. Subbaraos, Journal of Ovonic Research 12 (2016) 261-266.
35. S.K. Das, P.P. Rout, S.K. Pradhan, and B.K. Roul, Journal of Advanced Ceramics 1 (2012) 241-248.
36. R.L. Millard, R.C. Peterson, and B.K. Hunter, Am. Mineral. 80 (1995) 885-896.
37. A. Mebrek, S. Alleg, S. Benayache, and M. Benabdeslem, Ceram. Int. 44 (2018) 10921-10928.
38. A.C. Caballero, J.F. Fernández, C. Moure, P. Durán, and Y.M. Chiang, J. Am. Ceram. Soc. 81 (1998) 939-944.
39. F.X. Zhang, Y. Tong, K. Jin, H.B. Bei, W.J. Weber, and Y.W. Zhang, Entropy 20 (2018) 900:1-9.
40. K. Verma, S. Sharma, D.K. Sharma, R. Kumar, and R. Rai, Adv. Mater. Lett. 3 (2012) 44-50.
41. A. Moutaouaffiq, M. Belhajji, A. Rjeb, S. Sayouri, D.S. Houssaini, and T.D. Lamcharfi, J. Ceram. Process. Res. 23[5] (2022) 570-582.
42. H. Xu, L. Gao, and J. Guo, J. Eur. Ceram. Soc. 22 (2002) 1163-1170.
43. C. Mao, S. Yan, S. Cao, C. Yao, F. Cao, G. Wang, X. Dong, X. Hu, and C. Yang, J. Eur. Ceram. Soc. 34 (2014) 2933-2941.
44. H.T Dong, D.R. Jin, C.J. Xie, J.R. Cheng, J. Chen, and J.G. Chen, 2014 Joint IEEE International Symposium on the Applications of Ferroelectric, International Workshop on Acoustic Transduction Materials and Devices & Workshop on Piezoresponse Force Microscopy, 1-4 (2014).
45. C.S. Chou, C.H. Yang, P.Y. Lee, and Y.C. Lee, Mater. Chem. Phys. 242 (2020) 122569, 1-9.
46. Y.C. Lee and Y.L. Huang, J. Am. Ceram. Soc. 92 (2009) 2661-2667.
47. C. Rayssi, S.E. Kossi, J. Dhahri, and K. Khirouni, RSC Adv. 8 (2018) 17139-17150.
48. J. Zhang and R. Zuo, J. Am. Ceram. Soc. 99 (2016) 3343-334.